Article citation info:
Szwajca F, Gawrysiak C, Pielecha I. Effects of passive pre-chamber jet ignition on knock combustion at hydrogen engine. Combustion Engines. 2024;198(3):110-122. https://doi.org/10.19206/CE-189738

Filip SZWAJCA
Cezary GAWRYSIAK
Ireneusz PIELECHA

Combustion Engines
Polish Scientific Society of Combustion Engines

Effects of passive pre-chamber jet ignition on knock combustion at hydrogen engine

ARTICLE INFO

Received: 5 May 2024
Revised: 3 June 2024
Accepted: 6 June 2024
Available online: 3 July 2024

The use of gaseous fuels, including hydrogen, to fuel an engine enables an increase in efficiency and a significant reduction in toxic exhaust emissions. The research reported in this paper concerns a two-stage passive hydrogen combustion system for analyzing knock combustion under varying process conditions. The research was conducted using a single-cylinder AVL 5804 engine to determine the effect of the center of combustion (CoC) and excess air ratio (λ) on engine knock conditions and other engine parameters. The tests were carried out at a constant speed of n = 1500 rpm, variable CoC adjustments (2–18°CA aTDC), and a variable value of λ = 1.25–2.0. It was determined that at λ = 1.25–1.5, knocking combustion is quite intense, and further increases in λ this knocking are needed. The excess air ratio λ was found to have a much greater effect on the knock appearance in the engine than the center of combustion position.

Key words: *hydrogen combustion, turbulent jet ignition, knock combustion, knock indexes, thermodynamic indexes*

1. Introduction

1.1. Combustion of hydrogen in the internal combustion engines

The necessity to reduce fuel consumption is driving the exploration of new fuels or changes in the design of internal combustion engines. One substitute for fossil fuels is the use of hydrogen (a zero-emission fuel) and the use of a two-stage combustion system to increase the attractiveness of the internal combustion engine.

Hydrogen as a fuel allows the operation of an internal combustion engine in a wide range of excess air ratio (λ), from a highly enriched mixture to a very lean mixture, from 0.14 to 10 under conditions of 1 atm and 298 K [2]. This range of boundary values is due to the flammability limit of hydrogen in air of 4–76% [36]. The stoichiometric mixture during hydrogen combustion assumes a value of 34.5:1 (air to fuel) [36]. Under conditions of increased temperature in the combustion chamber and the following conditions: stoichiometric mixture, high load, speed characteristic of high power, and higher compression ratio, the probability of knock increases decisively – the difficult issue is its elimination [29].

Das [10] and White [35] analyzed the controllability of hydrogen combustion in an internal combustion engine and found that at $\lambda \geq 2$, NO_x concentrations can be reduced to less than 100 ppm without additional exhaust gas after treatment using, for example, a three-way catalytic reactor. Nagalingam [24] studied the exhaust emissions of a supercharged engine with a mechanical compressor at an intake system pressure of 2.6 bar and $\lambda > 2.5$ and evaluated NO_x concentrations below 100 ppm. Natkin [25] also evaluated the concentration of NO_x in the exhaust gas at $\lambda = 4$, which was 90 ppm. The same author, in a Ford engine powered by a mechanical compressor, conducted a hydrogen combustion process at $\lambda = 4.34$ and determined NO_x concentrations of 3–4 ppm [25].

In summary, it can be concluded that at $\lambda \geq 1.8$, the concentration of NO_x in the exhaust gas is significantly reduced, and this is done without additional systems such as a three-way catalytic reactor [33]. However, an unfavorable feature of lean mixtures is that the flame propagation rate is dramatically reduced as λ increases. In addition, with very lean mixtures, two spark plugs may be required.

Hydrogen as a fuel for the internal combustion engine is a promising step toward low-emission propulsion [14]. Harmful compounds formed in the combustion process are NO_x, the concentration of which can be controlled and even reduced to 3–4 ppm at specific engine operation points. Table 1 shows the properties of hydrogen, which are compared with other commonly used fuels such as CNG, gasoline, and diesel.

The heating value of hydrogen is 3 times that of gasoline and diesel fuel (at very low density). The minimum ignition energy indicates high flammability relative to the other fuels, and the laminar flame speed in the air is also 4 times greater than theirs. Gasoline and diesel fuels have narrow flammability limits (the window of the volumetric limit is about 6%). For CNG, this range is slightly wider (about 10%). However, for hydrogen, the flammability limit is 72%. On the other hand, the lower flammability limit for hydrogen in air is higher: it is 4%, which is higher than for gasoline (1%) and diesel (0.6%).

1.2. Combustion in the TJI system

The two-stage combustion technology, called TJI, was developed for Formula 1 by the German company Mahle [23]. Units equipped with this system have two chambers: a pre-combustion chamber and a main chamber. Control of the mixture concentration in both chambers requires an individual fuel supply for each chamber. The pre-chamber is called active when equipped with a fuel supply system or passive – in the absence of direct fuel injection into the pre-chamber. In the active configuration, a fuel dose of about 2–5% of the main dose is delivered to the pre-chamber. An indirect injection system delivers the rest of the fuel to the main chamber [5].

Table 1. Physical and chemical properties of hydrogen versus conventional fuels [36]

Property	Hydrogen	CNG	Gasoline	Diesel
Carbon content [% mass]	0	75 [e]	84	86
Lower heating value [MJ/kg]	119.7	45.8	44.8	42.5
Density [a,b] [kg/m^3]	0.089	0.72	730–780	830
Volumetric energy content [MJ/m^3]	10.7	33	33×10^3	35×10^3
Molecular weight	2.016	16.043 [e]	~110	~170
Boiling point [a] [K]	20	111 [e]	298–488	453-633
Auto-ignition temperature [K]	858	813 [e]	~623	~523
Minimum ignition energy in air [a,d] [mJ]	0.02	0.29	0.24	0.24
Stoichiometric air/fuel mass ratio	34.5	17.2 [e]	14.7	14.5
Stoichiometric volume fraction in air [%]	29.53	9.48	~2 [f]	–
Quenching distance [a,c,d] [mm]	0.64	2.1 [e]	~2	–
Laminar flame speed in air [a,c,d] [m/s]	1.85	0.38	0.37–0.43	0.37–0.43 [g]
Diffusion coefficient in air [a,b] [m^2/s]	8.5×10^{-6}	1.9×10^{-6}	–	–
Flammability limits in air [% vol.]	4–76	5.3–15	1–7.6	0.6–5.5
Adiabatic flame temperature [a,c,d] [K]	2480	2214	2580	2300

[a] at 1 bar, [b] at 273 K, [c] at 298 K, [d] at stoichiometry, [e] methane, [f] vapor and [g] n-heptane.

Combustion is initialized in the pre-chamber, which contains the injector and spark plug or the spark plug itself (passive system). Ignition of the mixture in the pre-chamber causes burning jets to pass through narrow channels into the main chamber, initializing the combustion of the lean fuel-air mixture. Such initialization is multi-point, so the mixture in the main chamber is ignited in several volumes simultaneously, resulting in rapid combustion of the main charge [5].

1.3. Purpose of the investigation

The main research problem of the present work is to expand knowledge in the following areas:

- evaluation of the hydrogen combustion thermodynamic characteristics as a function of the excess air ratio of the hydrogen-air mixture
- the effect of varying the center of combustion as a control parameter in hydrogen combustion
- occurrence of knock combustion in a hydrogen engine
- determination of mixture leanness and the center of combustion angle favoring the occurrence of knock combustion phenomenon.

The above research problems were solved using experimental tests on a single-cylinder research engine. Fast-varying processes and techniques were used to analyze the processes occurring in the combustion chambers of a hydrogen-powered engine.

2. Knock combustion

2.1. Essence of knock combustion

Knock combustion, also known as detonation combustion, is an undesirable phenomenon in an engine, resulting in decreased power and efficiency. Knock combustion can also cause the engine to run unevenly or lead to engine failure (caused by excessive stresses and temperatures exceeding these components' strength).

Knock combustion is a key topic due to very strict emission standards. This forces corporations to design powertrains that achieve maximum efficiency while maintaining optimal power and torque.

There are many reasons for the abnormal combustion process; however, spark knock and surface ignition are considered the most characteristic. It is worth noting that knock itself is understood as the sound associated with the self-ignition of the fuel-air mixture or part of it before the progressive form of the flame initiated by the ignition spark. A spark knock is a repetitive knock controlled by the ignition advance angle, which directly affects the intensity of this phenomenon. Heywood proposed this division and definition [15]. The division described above is very important from the point of view of engine control. In both cases, knock is identified; however, only in one of them is the engine control unit able – simply and quickly – to respond effectively. This is done by delaying the ignition advance angle, and thus, it is possible to reduce the intensity of the phenomenon or eliminate it altogether.

2.2. Conditions for the occurrence of knock combustion

The characteristic of knock combustion is the accompanying extremely sudden release of energy, which causes intense pressure changes in the cylinder. The sudden pressure changes introduce vibrations of significant amplitude into the combustion chamber and propagate to the entire engine structure [21]. It is assumed that this pressure amplitude during knock combustion in spark-ignition engines is 5–7 kHz [16]. There are scientific papers in which the authors extend this range to 20 kHz [7].

Knock combustion is very likely in the stoichiometric mixture area (Fig. 1). The research conducted by Szwaja et al. [31] was intended to force intense knock combustion. It was emphasized that in order to force this phenomenon, the compression ratio and stoichiometric mixture were selected accordingly.

The authors [31] present several factors that affect the occurrence of knock combustion. These factors are compression ratio, ignition timing, and air excess ratio λ. Any action to increase the pressure inside the combustion chamber increases the probability of knock combustion. In Figure 2, the dependence of the combustion chamber pressure intensification on the ignition timing is shown. Increasing the ignition advance increases the probability of knock

combustion. It is also worth noting that hydrogen is much more sensitive to changes in ignition advance than gasoline.

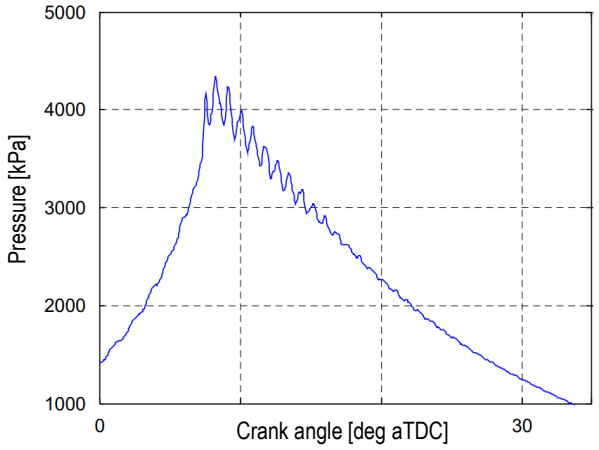

Fig. 1. Cylinder pressure with knocking combustion (ε = 12:1; n = 900 rpm; λ = 1) [31]

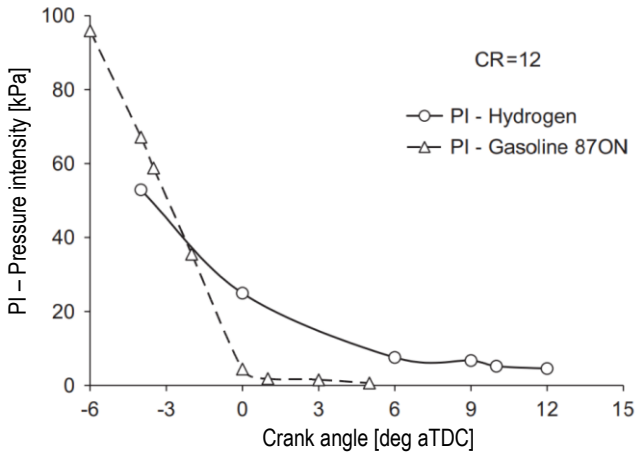

Fig. 2. Dependence of pressure intensification on ignition timing during hydrogen and gasoline combustion [31]

In summary, the first factor causing the knock combustion is use the stoichiometric mixture at which the phenomenon occurs. The next factor is the compression ratio. A compression ratio of 12 can be categorized as quite large for a range of spark-ignition engines. Units based on spark-ignition direct injection and equipped with supercharging are based on compression ratios of ε = 9.3 (e.g. VW 2.0 TFSI) and ε = 10.5:1 (e.g. VW 1.5 TSI EVO2). The last condition for the occurrence of knock combustion is the ignition advance. Karim [17] concludes that with hydrogen combustion in an internal combustion engine, optimizing the ignition advance is far more effective than with other fuels and allows for the control of knock combustion.

2.3. Detection methods for knock combustion

An index using the pressure pulsation maximum amplitude (MAPO) and another using the average value of the absolute pressure pulsation (IMPO) are the most commonly used knock indexes. Both indices rely on measuring the frequency of pressure in a cylinder with a high-pass filter [28]. Typical knock indices are shown below:

– MAPO – Maximum amplitude of pressure oscillations [6, 9, 13, 22]:

$$\mathrm{MAPO} = \max|p_{osc}| \tag{1}$$

where: p_{osc} – oscillatory component of combustion pressure;

– IMPO – integral modulus of pressure oscillations [3]:

$$\mathrm{IMPO} = \frac{1}{\theta_c}\int_0^{\theta_p}|p_{osc}|d\theta \tag{2}$$

where: θ_c – engine cycle time, θ_p – duration of the variable component p_{osc}, θ – crank angle;

– IMPOG – integral modulus of pressure oscillations gradient [11, 12]:

$$\mathrm{IMPOG} = \int_{\theta_{stp}}^{\theta_{stk}}\left|\frac{dp_{osc}}{d\theta}\right|d\theta \tag{3}$$

where: θ_{stp} – crank angle for knock start, θ_{stk} – crank angle for knock end;

– D3PDθ – maximum value from the third-order derivative of the pressure pulsation [8]:

$$\mathrm{D3PD\theta} = \max\left(\frac{d^3p_{osc}}{d\theta}\right) \tag{4}$$

– KI20 – Knock Index – indicator of knocking intensity in the window of 20°CA [19]:

$$\mathrm{KI20} = \sum_{i=1}^{n}\frac{(p_{osc}(i)-p_{av})^2}{\theta_{20}} \tag{5}$$

where: n – numbers of combustion cycles, $p_{osc}(i)$ – sample of the oscillatory component of the combustion pressure, p_{av} – average value of pressure oscillations, θ_{20} – number of samples in a window of width 20°CA.

Figure 3 shows a graphical representation of the indicators presented previously.

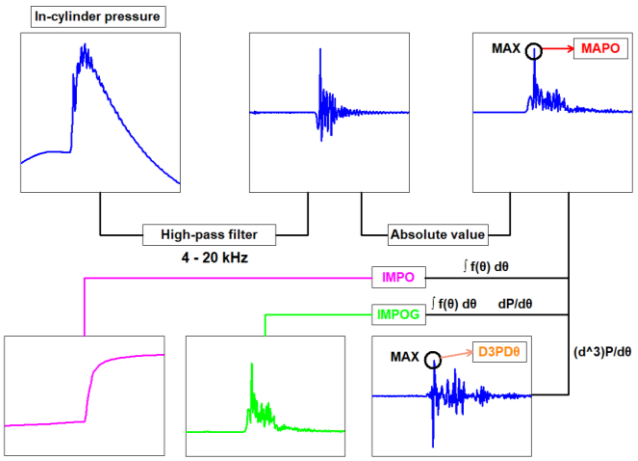

Fig. 3. Graphical representation of index calculation for MAPO, IMPO, IMPOG, and D3PDθ

2.4. Knock categorization

The limit for the occurrence of knock combustion at the MAPO index takes different values in the literature. Aramburu [1] conducted a study that used a 6-cylinder engine with a displacement of 5.883 dm^3 and adopted a MAPO limit value = 4 bar. Szwaja and Naber [32] adopted a limit value of MAPO = 0.1 MPa to distinguish be-

tween the correct mixture combustion process initiated by the spark plug and the combustion process initiated by the self-ignition of the mixture. They found that at the self-ignition of the mixture, the maximum pressure pulsations take values much higher than 0.1 MPa. The limit MAPO = = 1 bar [26, 30, 34] is the most widely accepted value to distinguish a correct combustion process from one in which knocking combustion has occurred.

The MAPO limit is a very individual indicator that takes on different values due to the displacement volume or compression ratio. Taking into account the displacement volume of the AVL 5804 engine of swept volume 0.5107 dm^3 and the fact that the most commonly accepted limit value in publications is MAPO = 1 bar, this work also adopts this value to identify the phenomenon of knock combustion.

3. Research methodology

3.1. Engine test bench

The tests were carried out using an AVL 5804 test unit (Fig. 4), which is a single-cylinder engine adapted for hydrogen combustion. The engine is equipped with a two-stage combustion system and a passive pre-chamber. The technical parameters of the engine are shown in Table 2.

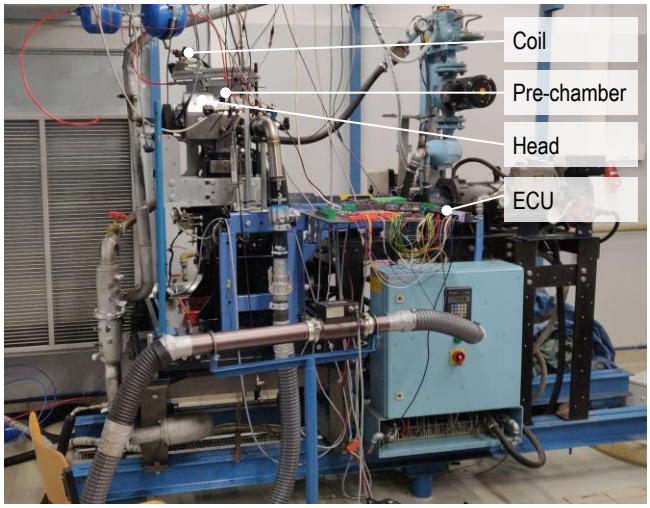

Fig. 4. AVL 5804 single-cylinder engine with TJI system

Table 2. Technical parameters of the AVL 5804 engine

Parameter	Unit	Value
Engine	–	1-cyl., 4-valve, SI, TJI
Cylinder volume	dm^3	0.5107
Bore	mm	85
Stroke	mm	90
Compression ratio	–	14.5:1
Air intake	–	supercharged

The pre-chamber was equipped with 6 radially distributed nozzles with a diameter of 1.7 mm leading to the main chamber. A spark plug is fitted in the pre-chamber. The volume of the pre-chamber is 6.6% of the main combustion chamber above the piston in the TDC. Fuel was supplied to the main chamber via an electromagnetic injector, located in the intake manifold.

3.2. Research apparatus

A schematic of the test stand and measuring apparatus is shown in Fig. 5. Hydrogen was supplied from a 40 dm^3 cylinder, in which the initial pressure of 150 bar was reduced to 6.5 bar (into the main chamber). In addition, two 2.5 dm^3 tanks (to reduce pressure pulsation) were mounted in front of the injector, connected in series. Fuel dose was calculated based on mass flow rate using a Bronkhorst 111B flow meter.

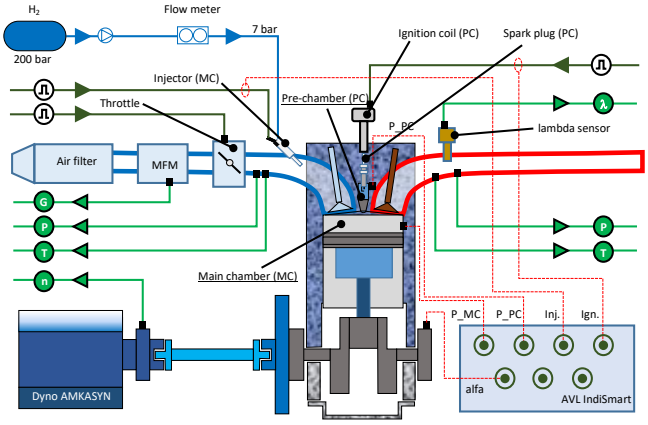

Fig. 5. Layout of engine and test apparatus

The start of hydrogen injection was fixed at 260°CA before TDC. Ignition and throttle position were controlled by Ecumaster's EMU Black controller. Adjustment of the throttle position by the mentioned controller made it possible to adjust the excess air ratio (a constant air overpressure of 1 bar was provided by an external mechanical compressor).

To analyze the combustion process, combustion pressures in the main chamber (AVL GH14D pressure sensor: 0–25 MPa) and pre-chamber (Kistler 6081 AQ22: 0–25 MPa) were recorded using AVL IndiSmart together with a crankshaft position sensor (AVL 364C01; 0.1 deg).

The excess air ratio was determined using IMFSoft's LCP80 controller and a Bosch LSU 4.9 wideband oxygen sensor (measurement range 0.7–12.5) mounted in the engine's exhaust system.

3.3. Scope of research

The tests were carried out at a constant engine speed of n = 1500 rpm, with different values of excess air ratio and a variable center of combustion CoC (CoC angle for 50% of the heat released). The IMEP value was the value resulting from the fuel dose at the specified adjustment λ. Table 3 shows the test plan.

Table 3. Variable and constant values during engine tests

No.	λ value	Throttle	CoC [α]		Fuel dose
	–	%	Start	End	mg/cycle
1	1.25	30	2	14	4.32
2	1.35	32	2	18	4.16
3	1.50	38			4.13
4	1.60	43			4.20
5	2.00	64			4.25

Research conducted by Qiang et al. [27] indicates similar values of the air excess ratio when using a passive combustion chamber (tests were conducted at λ = 1.8).

3.4. Research procedure

The recorded high-speed variable quantities are shown in Fig. 6. The measured quantities were analyzed using AVL Concerto software with an implemented library of calculation procedures.

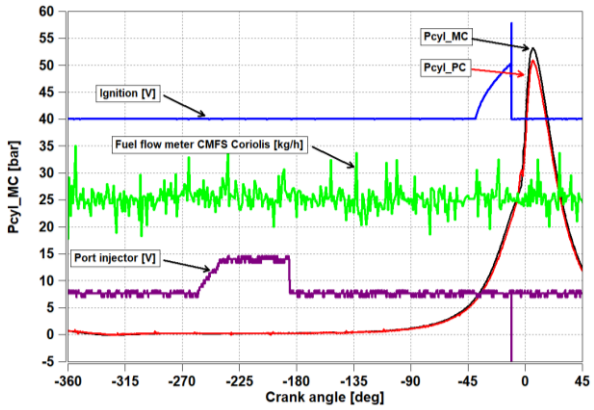

Fig. 6. Examples of parameters recorded during engine operation

The following parameters were analyzed:

– Averaged cylinder pressure from 100 post-measurement cycles:

$$P_{cyl}(\alpha) = \frac{\sum_{i=1}^{100} P_{cyl\_i}(\alpha)}{100} \quad (6)$$

where: P_{cyl} – in-cylinder pressure, α – crank angle;

– Incremental cylinder pressure dP_{cyl}

$$dP_{cyl}(\alpha) = \frac{dP_{cyl}(\alpha)}{d\alpha} \quad (7)$$

– Indicated mean effective pressure (IMEP):

$$IMEP = \frac{1}{V_s} \cdot \sum P_{cyl}(\alpha) \cdot dV \quad (8)$$

where: V_s – swept volume, V – actual cylinder volume;

– Heat rate released (dQ):

$$dQ/d\alpha = \frac{\kappa}{\kappa-1} \cdot P_{cyl}(\alpha) \cdot \frac{dV}{d\alpha} + \frac{1}{\kappa-1} \cdot V \frac{dP_{cyl}(\alpha)}{d\alpha} \quad (9)$$

where: κ – specific heat ratio $\left(\frac{c_p}{c_v}\right)$;

– Heat released (Q):

$$Q = \int_{SOC}^{EOC} \frac{dQ}{d\alpha} dv \quad (10)$$

where: SOC – start of combustion, EOC – end of combustion;

– Ni – indicated power

$$N_i = \frac{V_s \cdot IMEP \cdot n}{\tau} \quad (11)$$

where: n – engine speed, τ – engine cyclicality.

4. Experimental row results

The basic parameter and also the most important carrier of information about the conditions in the combustion chamber is the pressure in the cylinder. Examples of pressure waveforms in the main chamber (MC) and pre-chamber (PC) are shown in Fig. 7.

The variation of CoC position was achieved by changing the ignition timing advance (Fig. 8). Changes in CoC were made in increments of ΔCoC = 2°CA (ignition angle was adjusted to obtain the correct CoC value). At λ = 1.25 the CoC was changed in the range of 2–14°CA aTDC, at the other test points 2–18°CA aTDC.

a)

b)

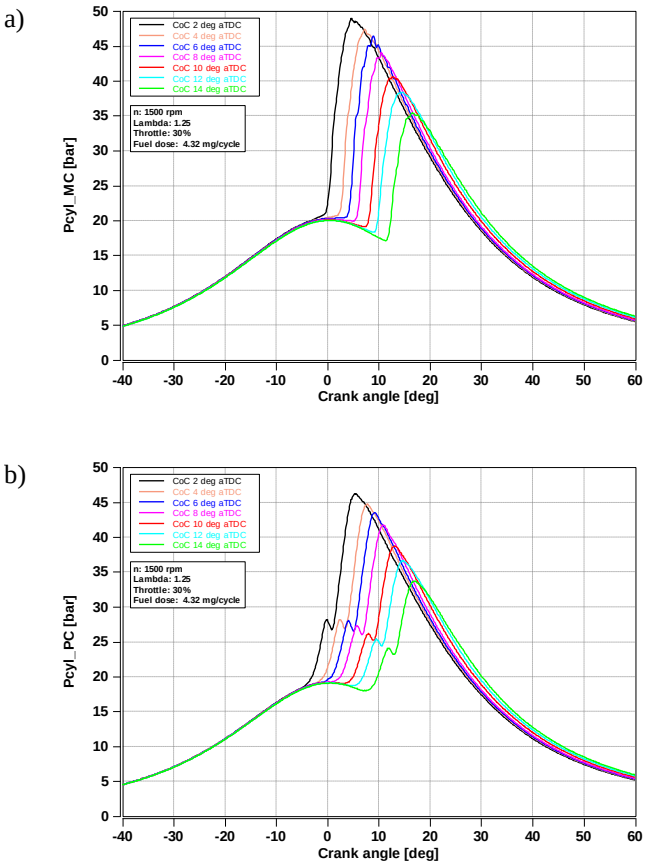

Fig. 7. Example of cylinder pressure waveform with λ = 1.25 and different CoC = 2–14°CA aTDC: a) in main chamber; b) in pre-chamber

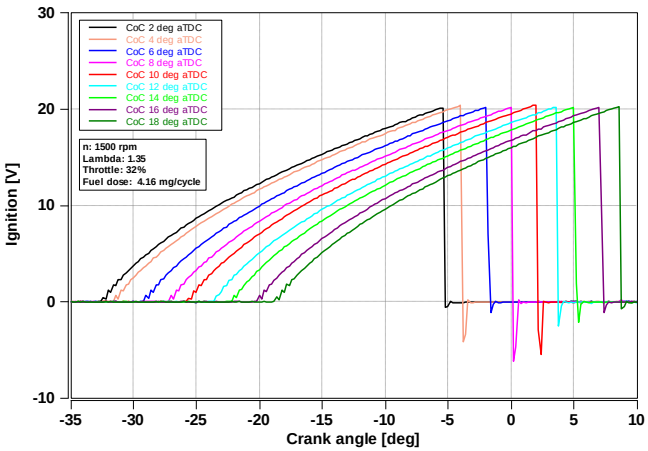

Fig. 8. Current in the primary circuit of the ignition coil for different values of CoC at the λ = 1.35

A complete center of combustion analysis as a function of ignition timing is shown in Fig. 9. It shows that as the

excess air ratio increases, obtaining the same combustion centers requires more ignition advance. At λ = 1.25, achieving CoC = 10°CA aTDC requires ignition at SOI = 2–3°CA aTDC. However, at λ = 1.5, the same CoC angle already requires an ignition advance of 2–3°CA (to SOI = 0°CA). Further increasing the excess air ratio to λ = 2 results in CoC = 10°CA aTDC, requiring a further ignition advance of 3°CA to a value of SOI = 3°CA bTDC.

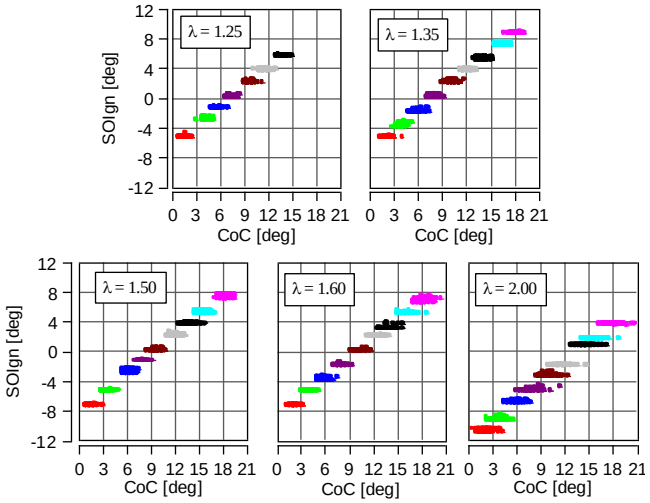

Fig. 9. Values of the ignition timing relative to the center of combustion CoC for all lambda λ values analyzed

In simulation studies conducted by Aljabri et al. [2], similar pressure curves were obtained in the cylinder and in the pre-chamber. The tests were carried out using a similar geometry of the combustion system (ε = 14.5), but with higher values of the excess air coefficient (λ > 2.8).

5. Combustion process thermodynamic indicators evaluation

5.1. Cylinder pressure

By delaying the CoC, the maximum pressure value in the combustion chambers is reduced. At each excess air ratio, the maximum value of combustion pressure in both chambers is reached at CoC = 2°CA aTDC, while the lowest pressure value occurs at the highest value of CoC: at λ = = 1.25 – CoC = 14°CA aTDC, and for other values of excess air ratio at CoC = 18°CA aTDC.

Further, an interesting relationship at different excess air ratios and different values of CoC angles was observed in the peak angular window of the main combustion phase. The part of the combustion process in point is presented in Fig. 10, which shows a narrow angular window for successively the richest and the leanest mixture. The different rates of pressure rise after ignition can be seen. Tap burning occurs at virtually any value of CoC (at λ = 1.25), which is not observed at λ = 2.0.

Similar changes (decrease in P_{mx} – from 23 to 16 bar at CoC = 1–15 deg aTDC). depending on CoC was reported in the study by Qiang et al. [27] (research was carried out at n = 1600 rpm and λ = 1.8).

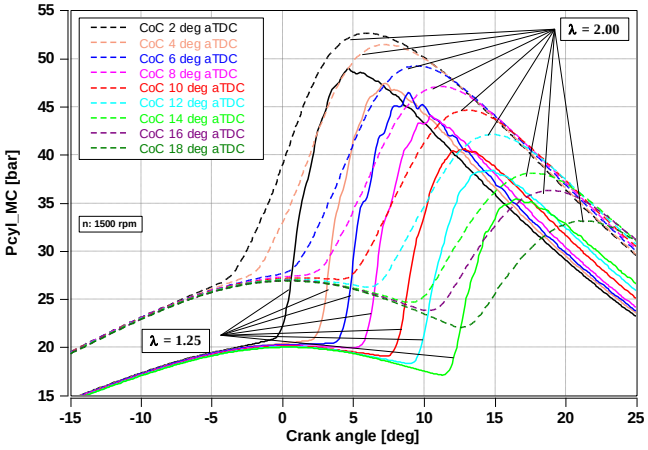

Fig. 10. Cylinder combustion pressure for λ = 1.25 and λ = 2.00 at the full range of CoC values analyzed

The relationship of pressure rise in both chambers at λ = = 1.25 is shown in Fig. 11a. A rapid increase in pressure is observed, suggesting that the combustion process was assisted by knocking combustion. At CoC = 2–8°CA aTDC, very significant pressure increments are observed. With further increases in CoC, dP_{cyl} values decrease. Despite the smaller maximum values, knock combustion was still observed.

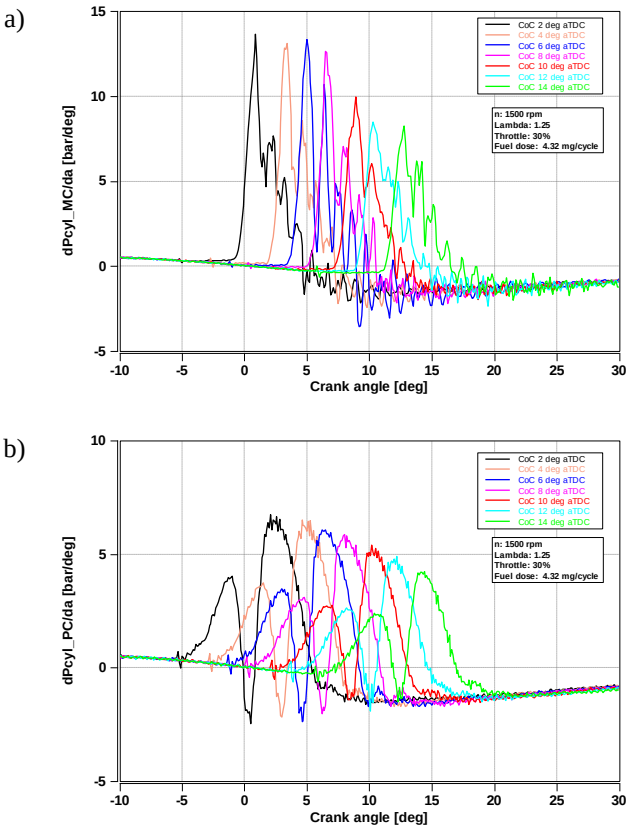

Fig. 11. Pressure rise rate for λ = 1.25 at the full range of analyzed CoC values in a) cylinder, b) pre-chamber

Figure 11b shows the same pressure rise changes in the pre-chamber. Such rapid changes as in the cylinder are not

observed, but there is also knocking combustion. It can be seen that the pressure rise peaks characteristic of two-stage combustion with a pre-chamber is reached twice.

Figure 12 shows the combustion pressure P_{cyl} in both chambers (Fig. 12a) and the pressure rise $dP_{cyl}/d\alpha$ at λ = = 1.35 (Fig. 12b).

The pressure difference between the chambers is a feature of the two-stage combustion system and inter-chamber throttling. Regardless of the CoC value, an increased pressure value in the pre-chamber is observed when the mixture is ignited around the spark plug (Fig. 12a). Subsequently, the burning charge in the pre-chamber is transferred to the main chamber, causing combustion to begin in the cylinder. In the MC chamber, higher pressure values are obtained regardless of the CoC change.

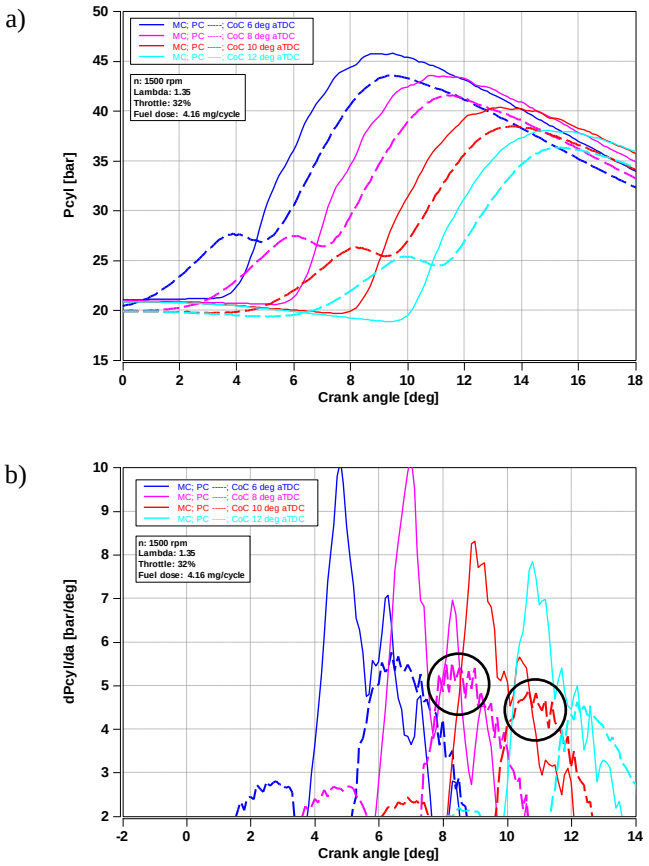

Fig. 12. Cylinder pressure P_{cyl} (a) and pressure rise $dP_{cyl}/d\alpha$ (b) at λ = 1.35 and CoC = {6, 8, 10, 12°CA} in a narrow window of crankshaft angle

Analyzing the pressure rise rate in both chambers $dP_{cyl}/d\alpha$ (Fig. 12b), some oscillations (also present in Fig. 11b) can be observed, which do not indicate knock combustion. This is due to the values of these oscillations. They may be due to the lack of filtering of the measurement signal. As mentioned earlier, it was assumed that knock combustion is characterized by oscillations of 1 bar, and here a maximum of Δp = 0.2 bar was obtained.

5.2. Indicated mean effective pressure

Indicated mean effective pressure (IMEP) is a basic thermodynamic indicator that is a measure of operating efficiency for engine displacement. Figure 13 shows the IMEP values for both combustion chambers depending on CoC. The IMEP in the pre-chamber is lower than that in the main chamber. This is due to the previously described pressure and charge flow dependency.

It was observed that at two values of excess air ratio λ = = 1.25 and λ = 1.35, the trend of IMEP change increased with each successive CoC position. There is no decreasing trend due to the absence of successively higher CoC values (due to lack of combustion or very high ignition dropout). At the aforementioned excess air ratio values, IMEP takes on a maximum value of 3.79 and 3.96 at CoC = = 14°CA aTDC and CoC = 18°CA aTDC angles in the main chamber. The situation is slightly different in more dilute mixtures. At λ = 1.50 and λ = 2.00, the peak IMEP occurs at CoC = 12°CA aTDC in the MC. In contrast, at λ = = 1.60, the maximum value of 4.27 occurs at CoC = {8, 10, 12°CA} in MC.

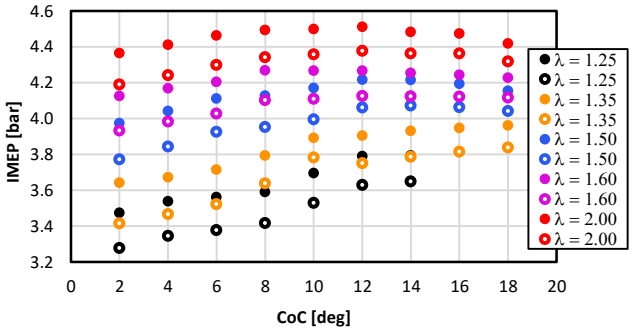

Fig. 13. The value of the indicative mean effective pressure as a function of the center of combustion for the main and pre-chamber (● – MC, ○ – PC)

Research conducted by Attard et al. [4] indicate that maximum brake torque (MBT) falls within the combustion center angle of 6–9 deg aTDC. They also define knocking combustion limits: for fuels with a high octane number (FON) the CoC limit is 2 deg aTDC (at FON = 96). The knocking combustion limit shifts towards higher CoC values with a limited fuel octane number (at FON = 75, the CoC limit is 20 deg aTDC).

The maximum IMEP value occurs at λ = 2.00 in each of the analyzed CoCs, which correlates with the benefits of lean combustion. The IMEP increases each time the mixture dilution increases, starting at λ = 1.25, for which it assumes the lowest values. This situation is due to the fact that the increase in charge dilution was realized by increasing the amount of air and not by reducing fuel dosing. Such adoption of the test methodology was due to the requirement to ensure a constant flow of hydrogen (limiting the possibility of reducing the hydrogen injection time).

Moreover, it is worth looking at the difference between the IMEP in the main chamber and the pre-chamber, as presented in Fig. 14. The difference between the IMEP values in the two chambers successively decreases with increasing CoC regardless of the value of λ. Such a condition can be explained by long-duration combustion leading to a decrease in differences in both chambers. Mild anomalies were noted at λ = 1.35 and CoC = {8, 10°CA}, where

the function strongly deviates from the other excess air ratios.

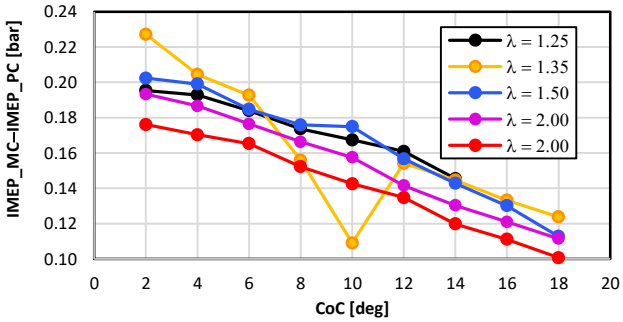

Fig. 14. IMEP difference between MC and PC chambers as a function of CoC

5.3. Heat release characteristics

Heat release analysis was carried out according to the thermodynamic index equations presented in subsection 4.4.

Figure 15 shows the heat release curves in the main chamber for all CoCs and selected curves in the pre-chamber for successively the smallest, middle and largest CoC angle for the excess air ratio λ = 1.25. A decrease in the heat release results in a certain maximum. Such a pattern may suggest a rapid loss of heat to the walls whose temperature, due to the hydrogen supply, was significantly reduced.

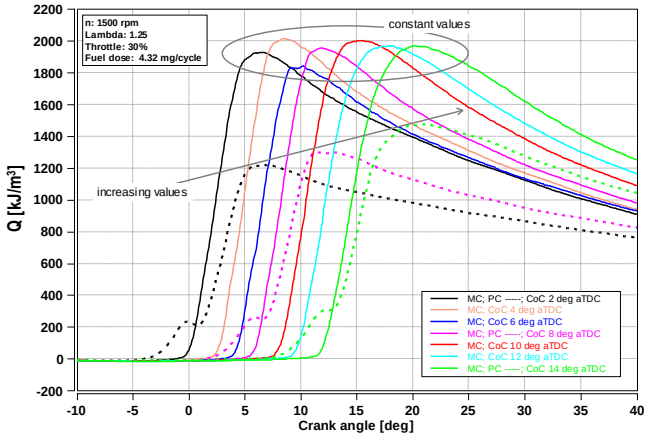

Fig. 15. Heat released in the main chamber and pre-chamber at different values of CoC and λ = 1.25

It is observed that at CoC = {8, 12, 14°} the course of heat release in the main chamber is similar, this also applies to the maximum values. The analysis of Q in the main chamber shows an increasing value of the maximum heat release with the delay of CoC. It means that delaying the CoC positively affects the quality of combustion in the pre-chamber. Such a delay in CoC (and thus ignition) is conducive to improving the quality of the charge accumulated in the pre-chamber.

In addition, as the CoC increases, the difference between the maximum values in the main chamber and the pre-chamber decreases, due to the increasing maximum values of the amount of heat released in the pre-chamber.

An analysis of the maximum amount of heat released for a number of λ and CoC variants is shown in Fig. 16. It shows that an increase in λ results in a decrease in the maximum amount of heat in the main chamber. In the pre-chamber, regardless of λ and CoC, the heat value is significantly lower.

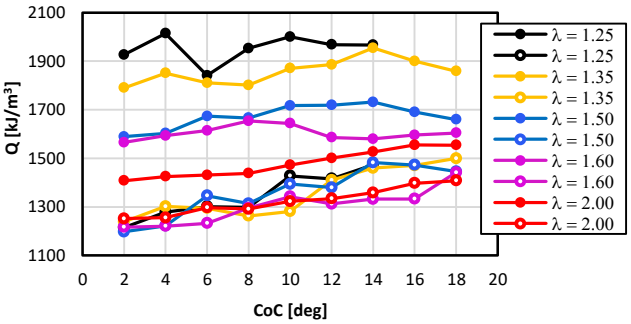

Fig. 16. Maximum values of heat released at different excess air coefficients as a function of CoC (● – MC, ✪ – PC)

Analysis of the heat release rate shows that there are dependencies related to λ and CoC (Fig. 17). At a constant λ, increasing CoC by 6°CA causes the maximum of the heat release rate to shift by about 5°CA. Increasing λ causes much smaller values of dQ/dα to be observed at the same CoC with a simultaneous acceleration of about 2°CA. Changing λ from 1.25 to 2.0 causes the heat release rate to be reduced by 3 times regardless of CoC.

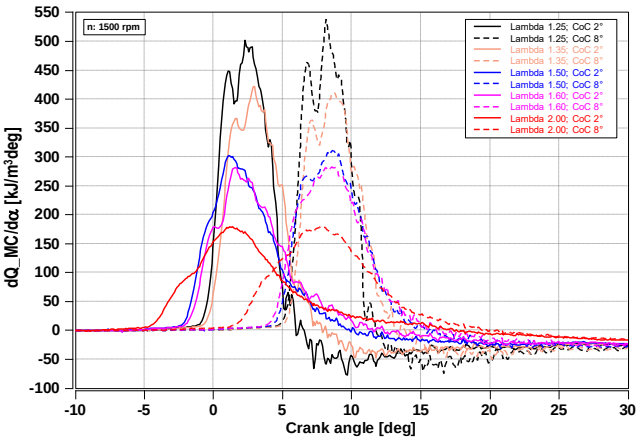

Fig. 17. Heat release rate for CoC 2° and 8°CA and all analyzed values λ

The last thermodynamic indicators analyzed in this section are HR10 – the start of combustion (defined as the angle at which 10% of the heat is released) and HR90 – the end of combustion (defined as the angle at which 90% of the heat is released), which are presented in Fig. 18. The difference between these two thermodynamic indicators is the combustion duration HR90–HR10. At λ = 1.25, the start of the combustion follows CoC. At the maximum value of CoC, maximum IMEP is observed. Similar parameters were observed at λ = 1.35. The start of combustion ranges from 6 to 8°CA. Further increasing the value of λ results in a characteristic maximum IMEP. $IMEP_{mx}$ values occur in the range of CoC = 8–12°CA aTDC at high values of λ. At

λ = 2.00, the combustion time increases and is about 10°CA.

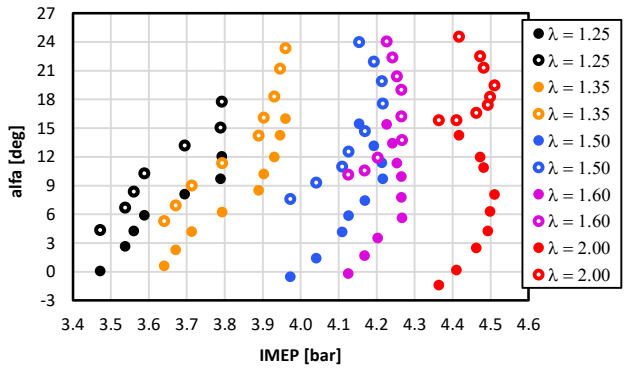

Fig. 18. The angle of 10% HR10 and HR90 90% of the heat released relative to IMEP (● – HR10, ○ – HR90)

Concluding the analysis in this section, the combustion durations were tabulated (Fig. 19). It was observed that for excess air ratios λ = 1.25 and 1.35, increasing the CoC angle increases the combustion time. It has to do with delaying the beginning of combustion and, at the same time, ending it later. The maximum combustion time with higher CoC values is increased at both λ values. At λ = 1.5 and 1.6, almost constant combustion duration values are observed, averaging 9°CA. Combustion conditions at λ = 2.0 cause the combustion time to decrease with increasing CoC. At CoC = 2°CA, the combustion time was 17°CA, and at CoC = 18°CA aTDC decreased to 10°CA. The combustion time values are consistent with the results of Wang et al. [34], who, at λ = 2.0 (for a supercharged DISI engine without a two-stage combustion system), obtained a combustion time of 15°CA (keeping CoC in the range of 8–9.7°CA aTDC).

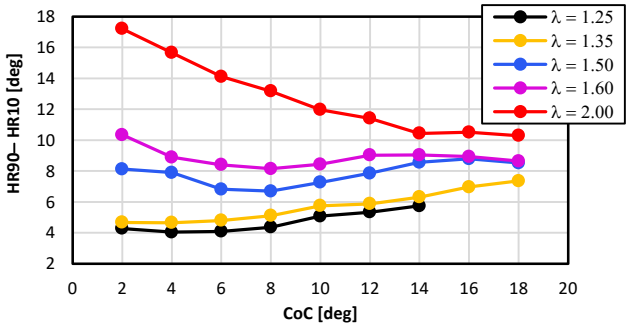

Fig. 19. Combustion duration HR90-HR10 relative to CoC

Research conducted by Qiang et al. [27] (λ = 1.8) indicates a similar trend (slow increase) of combustion time in the range of λ = 1.25–1.6. The author's own research found that at λ = 2.0, the trend is reversed.

5.4. Engine performance indicator

Indicated power is shown in Fig. 20 as a function of variable CoC and variable excess air ratio. It is observed that the indexed power increases with the dilution of the mixture. The analysis in terms of the changing CoC is no longer clear. At λ = 1.25 and λ = 1.35 each time, the indicated power increases with increasing CoC. For successive values of excess air coefficients, the indicated power value reaches a maximum in the range CoC = 8–12°CA aTDC. At λ = = 2.0, the indicated power is highest at CoC = 12°CA aTDC.

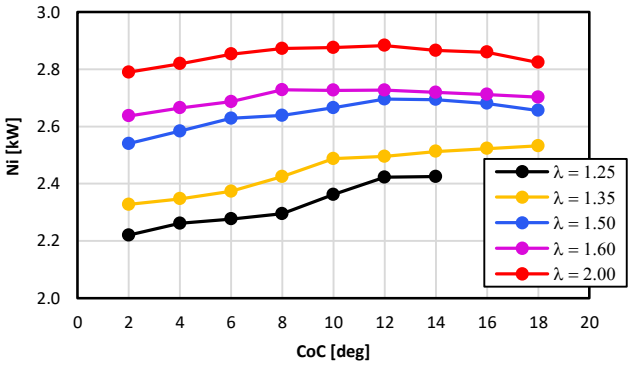

Fig. 20. Indicated power Ni relative to CoC

6. Knock combustion indicators

Equation (1) presents the maximum amplitude of pressure pulsation (MAPO). The MAPO values were determined by measuring the indicated pressure in both chambers. Then, the measured pressure is subjected to filtering using a high-pass filter. The frequency analysis range is 4–20 kHz in the window of 0–70°CA with a measurement resolution of 0.1° increments. Figure 21 below shows the measured pressure in the main and pre-chamber and the resulting function after filtering in a narrowed window of 0° to 30°CA.

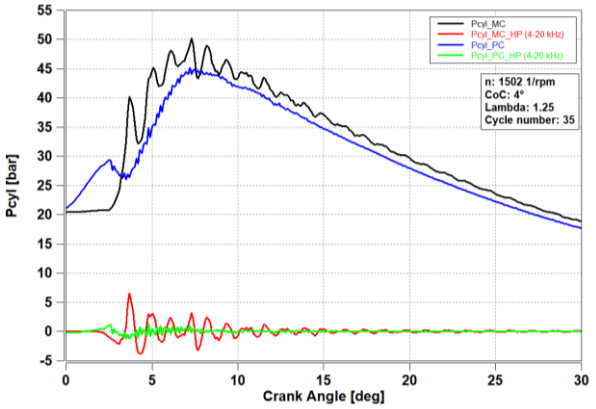

Fig. 21. The effect of using a high-pass filter. Pressure waveform in the cylinder (black line) and pre-chamber (blue line) along with the filtered part – red line (cylinder), green line (pre-chamber)

The next step was to calculate the value of the maximum pulsation in both chambers (red and green lines in Fig. 21). This maximum value is the MAPO knock index, which was presented for the main chamber (Fig. 22) and for the pre-chamber (Fig. 23). It was observed that at λ = 1.25 the knock is most intense with a maximum value of MAPO = 7.996 bar for cycle number 95 and CoC = 8°CA aTDC. In total, only five cycles exceeded the 7 bar pressure oscillation value. At λ = 1.25, it was noted that CoC in the range of 2–6°CA aTDC resulted in similar knock combustion

patterns (similar MAPO distributions in Fig. 22a). Further retardation of the CoC causes the maximum knock intensity to decrease (but far exceeds the 1 bar limit). At $\lambda = 1.35$, similar characteristics were observed – but the maximum knock mostly does not exceed 5 bar (Fig. 22b). The most intense knock occurred at CoC = 6°CA aTDC. Then, there was a slight reduction in the intensity of the phenomenon. However, further on, the appearance of knock combustion is undeniable. The next level of mixture dilution – $\lambda = 1.50$ – reduced the intensity of knocking to MAPO = = 3 bar (Fig. 22c). A further increase in $\lambda > 1.60$ (Fig. 22d, e) again reduced the intensity of knock combustion. The great majority of measurement cycles exceeded the limit MAPO = 1 bar. However, only a few cycles took values ≥ 2 bar. In the case of the last excess air ratio, $\lambda = 2.00$, the knock combustion phenomenon did not occur, as MAPO takes values < 1 bar (Fig. 22e).

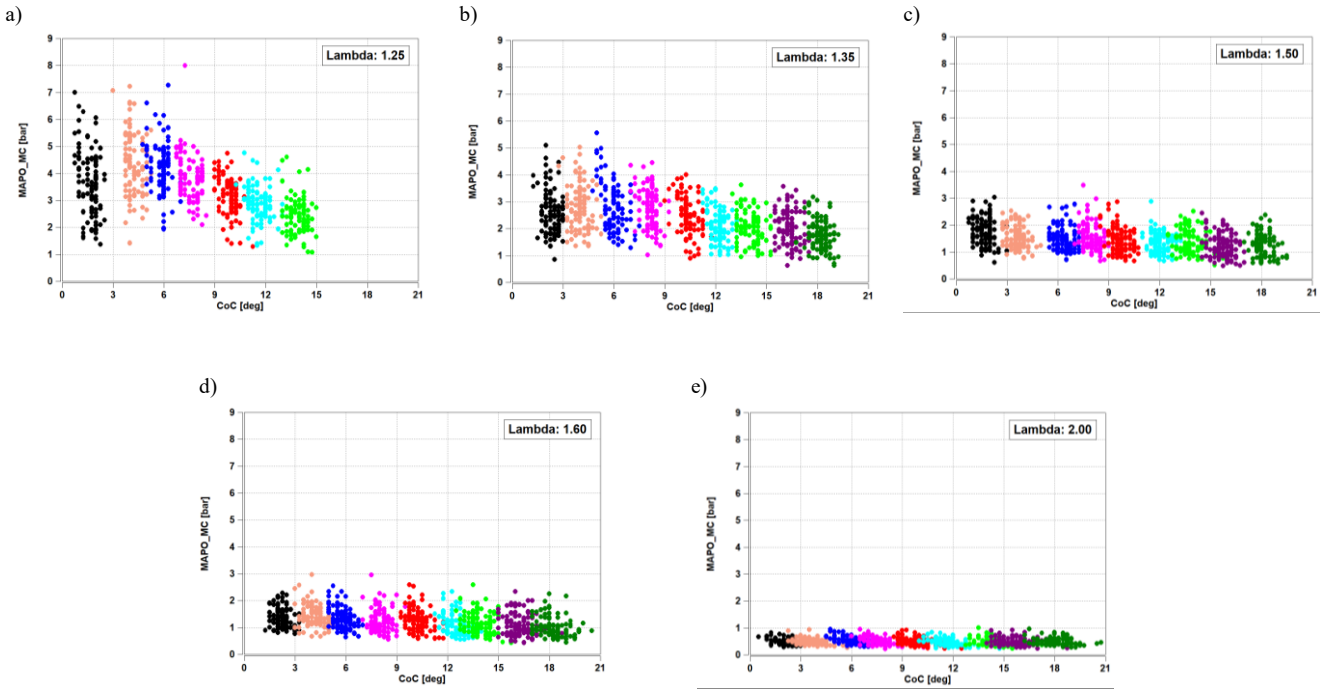

Fig. 22. Dependence of MAPO knock at different excess air ratios in the main chamber as a function of CoC

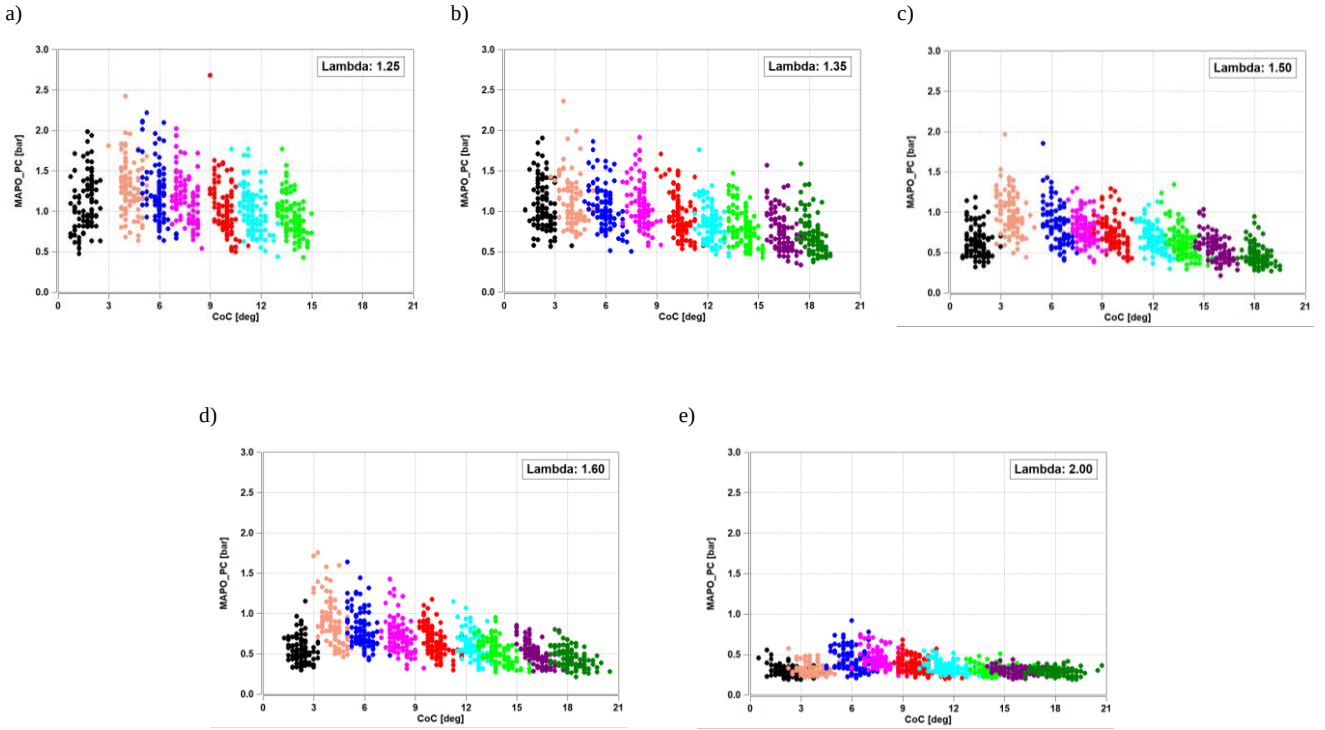

Fig. 23. Dependence of MAPO knock at different excess air ratios in the pre-chamber as a function of CoC

The MAPOs characterizing the pre-chamber are much smaller relative to those corresponding to the main chamber. At $\lambda = 1.25$, the maximum value of MAPO = 2.68 bar was obtained for CoC = 10°CA aTDC (Fig 23a). At $\lambda =$ = 1.35, and with a change in CoC, continuous knocking conditions (MAPO > 1 bar) are observed – Fig. 23b. At $\lambda =$ = 1.50 and $\lambda = 1.6$, the MAPO value did not exceed 2 bar, with most cycles reaching values below the MAPO = 1 bar limit (Fig. 23c) – corresponding to correct combustion (no knocking). As in the case of the main chamber, the entire measurement series at $\lambda = 2.00$ did not exceed the value of 1 bar, so combustion in the pre-chamber proceeded without the occurrence of knocking combustion. In addition, in the case of the leanest mixture, a slight increase in the maximum amplitude of pressure pulsations was noted at CoC = = 6°CA and CoC = 8°CA, but their value did not exceed 1 bar.

The reason for the reduction in maximum MAPO in the pre-chamber relative to the main chamber is twofold.

First, most of the charge is burned in the main chamber, where there is better purging from residual exhaust gas. Second, the pre-chamber volume is many times smaller than the main chamber. Knocking combustion occurs when there is a much more sudden heat release than in the case of a correct combustion process. Due to the intensification of pressure and the non-uniform nature of its distribution, pressure waves or shock waves are created, which then propagate through the chamber [15]. The lower intensity of this phenomenon in the pre-chamber is due to the smaller volume of the chamber, in which these shock waves do not develop to the same extent as in the main chamber.

Sun et al. [30] conducted tests using an SI engine without a pre-chamber and indicated that much higher ignition advance angle values were required to achieve knocking combustion (above 30 deg bTDC). In the current tests, an ignition angle of 5 deg bTDC caused very significant knocking combustion (at λ values < 2.0).

7. Conclusions

Investigations of the hydrogen combustion process using a two-stage combustion architecture under knock combustion conditions were carried out with lean mixtures in the range of $\lambda = 1.25$ to 2.0. It was found that under two-stage combustion conditions up to $\lambda = 1.6$, we are dealing with knock combustion. Under the analyzed conditions, a significant reduction is possible only by increasing the excess air ratio. Despite the fact that the research was conducted under conditions of limited IMEP loading, knock ranges were obtained that are in line with other studies [18, 20]. The main conclusions of the study are presented below.

1. Maintaining a constant CoC with increasing excess air requires increasing the ignition advance due to the extension of the combustion process.
2. The CoC delay results in a decrease of the maximum combustion pressure in the preliminary and main combustion chambers. In the analyzed range of CoC, the highest combustion pressure occurred at CoC 2°CA aTDC while the lowest occurred at the center of combustion fixed furthest from TDC, that is, at $\lambda = 1.25$ – CoC = 14°CA aTDC and for the remaining values of the excess air ratio at CoC = 18°CA aTDC.
3. At high values of excess air ratio, the maximum IMEP value was obtained at CoC = 12°CA aTDC. Analysis of the IMEP difference in both chambers indicates that increasing CoC reduces the IMEP difference in both chambers. The IMEP difference values for both combustion chambers decrease twice at extreme CoC setpoints.
4. The dependence of the combustion duration on the applied mixture composition and the position of CoC is shown. For mixtures in the range of $\lambda = 1.25$–1.35, the combustion time increases with the delay of CoC; increasing the dilution of the mixture to the value of 1.5 and 1.6 is characterized by the absence of significant differences in combustion time with changing CoC. For $\lambda = 2.00$, delaying CoC results in shorter combustion times.
5. The quantification of the knock combustion phenomenon is presented based on the MAPO index. The excess air ratio is a factor that affects knock much more significantly than changing the CoC. At small values of $\lambda =$ = 1.25–1.6, knocking occurs regardless of the CoC setting with a maximum value of MAPO ~ 7. Increasing the CoC over this range λ slightly reduces the intensity of knocking. At $\lambda = 2.0$, no knocking combustion (MAPO up to 1 bar) is observed over the entire CoC range.
6. Pre-chamber combustion analysis indicates the occurrence of knock in the range $\lambda = 1.25$–1.6. In this range, knock in the pre-chamber is characterized by three times lower MAPO values. At $\lambda = 2$, MAPO averages about 0.5 bar.

The presented research and analysis results do not exhaust the subject matter. Further research work will focus on:

- analyzes hydrogen knock combustion in terms of the active combustion chamber with a variable excess air ratio
- assessment of the ammonia combustion process in the TJI system as a zero-emission fuel
- co-combustion of hydrogen (injected into the pre-chamber) and ammonia (injected into the main chamber) in terms of knock combustion, excess air coefficient, and engine efficiency.

Acknowledgements

This work was supported by the Poznan University of Technology [interdisciplinary grant 0415/SIGR/7286].

Nomenclature

aTDC	after top dead center
bTDC	before top dead center
CNG	compressed natural gas
CoC	center of combustion
dPcyl	pressure rise rate
dQ	heat rate released

D3PDθ maximum value from the third-order derivative of the pressure pulsation
EOC end of combustion
FON fuel octane number
HR10 the start of combustion (angle at which 10% of the heat is released)
HR90 – the end of combustion (angle at which 90% of the heat is released)
IMEP indicated mean effective pressure
IMPO integral of modulus of pressure oscillations
IMPOG integral modulus of pressure oscillations gradient
KI20 Knock Index – indicator of knocking intensity
MAPO maximum amplitude of pressure oscillations
MBT maximum brake torque
MC main chamber
n engine speed
Ni indicated power
NO_x nitrogen oxides
Pcyl cylinder pressure
PC pre-chamber
PI pressure intensity
Q heat released
SOC start of combustion
SOIgn start of ignition
TDC top dead center
TJI Turbulent Jet Ignition
λ air excess ratio

Bibliography

[1] Aramburu A, Guido C, Bares P, Pla B, Napolitano P, Beatrice C. Knock detection in spark ignited heavy duty engines: an application of machine learning techniques with various knock sensor locations. Measurement. 2023;224:113860. https://doi.org/10.1016/j.measurement.2023.113860

[2] Aljabri H, Silva M, Houidi MB, Liu X, Allehaibi M, Almatrafi F et al. Comparative study of spark-ignited and pre-chamber hydrogen-fueled engine: a computational approach. Energies. 2022;15(23):8951. https://doi.org/10.3390/en15238951

[3] Arrigoni V, Cornettti G, Gaetani B, Ghezzi P. Quantitative systems for measuring knock. P I Mech Eng. 1972;186(1): 575-583. https://doi.org/10.1177/002034837218600137

[4] Attard WP, Blaxill H, Anderson EK, Litke P. Knock limit extension with a gasoline fueled pre-chamber jet igniter in a modern vehicle powertrain. SAE Int J Engines. 2012;5(3): 1201-1215. https://doi.org/10.4271/2012-01-1143

[5] Attard WP, Parsons PA. Normally aspirated spark initiated combustion system capable of high load, high efficiency and near zero NO_x emissions in a modern vehicle powertrain. SAE Int J Engines. 2010;3(2):269-287. https://doi.org/10.4271/2010-01-2196

[6] Benson G, Fletcher EA, Murphy TE, Scherrer HC. Knock (detonation) control by engine combustion chamber shape. SAE Technical Paper 830509. 1983. https://doi.org/10.4271/830509

[7] Brecq G, Le Corre O. Modeling of in-cylinder pressure oscillations under knocking conditions: Introduction to pressure envelope curve. SAE Technical Paper 2005-01-1126. 2005. https://doi.org/10.4271/2005-01-1126

[8] Checkel MD, Dale JD. Pressure trace knock measurement in a current S.I. production engine. SAE Technical Paper 890243. 1989. https://doi.org/10.4271/890243

[9] Chun KM, Heywood JB. Characterization of knock in a spark-ignition engine. SAE Technical Paper 890156. 1989. https://doi.org/10.4271/890156

[10] Das L. Hydrogen engines: a view of the past and a look into the future. Int J Hydrogen Energ. 1990;15(6):425-443. https://doi.org/10.1016/0360-3199(90)90200-I

[11] Ferraro CV, Marzano M, Millo F, Bochicchio N. Comparison between heat transfer and knock intensity on statistical basis. SAE Technical Paper 962101. 1996. https://doi.org/10.4271/962101

[12] Ferraro CV, Marzano M, Nuccio P. Knock limit measurement in high speed SI engines. SAE Technical Paper 850127. 1985. https://doi.org/10.4271/850127

[13] Franklin ML, Murphy TE. A study of knock and power loss in the automotive spark ignition engine. SAE Technical Paper 890161. 1989. https://doi.org/10.4271/890161

[14] Gis M, Gis W. The current state and prospects for hydrogenisation of motor transport in Northwestern Europe and Poland. Combustion Engines. 2022;190(3):61-71. https://doi.org/10.19206/CE-144560

[15] Heywood JB. Internal combustion engine fundamentals. 2nd ed. McGraw-Hill Education. New York 2018.

[16] Horner TG. Knock detection using spectral analysis techniques on a Texas Instrument TMS320 DSP. SAE Technical Paper 960614. 1996. https://doi.org/10.4271/960614

[17] Karim G. Hydrogen as a spark ignition engine fuel. Int J Hydrogen Energ. 2003;28(5):569-577. https://doi.org/10.1016/S0360-3199(02)00150-7

[18] Koch DT, Sousa A, Bertram D. H2-engine operation with EGR achieving high power and high efficiency emission-free combustion. SAE Technical Paper 2019-01-2178. 2019. https://doi.org/10.4271/2019-01-2178

[19] Konig G, Sheppard CGW. End gas autoignition and knock in a spark ignition engine. SAE Technical Paper 902135. 1990. https://doi.org/10.4271/902135

[20] Korn T, Ebert T, Vonnoe M, Tala H, Lang M. Hydrogen engines strong case – new performance benchmarks with hydrogen direct injection. 43rd International Vienna Motor Symposium. Vienna 2022.

[21] Lasocki J. Engine knock detection and evaluation: a review (in Polish). Zeszyty Naukowe Instytutu Pojazdów. 2016;109:41-50.

[22] Leppard WR. Individual-cylinder knock occurrence and intensity in multi-cylinder engines. SAE Technical Paper 820074. 1982. https://doi.org/10.4271/820074

[23] MAHLE Jet Ignition. https://www.mahle-powertrain.com/en/experience/mahle-jet-ignition/ (accessed on 10 April 2024)

[24] Nagalingam B, Dübel M, Schmillen K. Performance of the supercharged spark ignition hydrogen engine. SAE Technical Paper 831688. 1983. https://doi.org/10.4271/831688

[25] Natkin RJ, Tang X, Boyer B, Oltmans B, Denlinger A, Heffel JW. Hydrogen IC engine boosting performance and NO_x study. SAE Technical Paper 2003-01-0631. 2003. https://doi.org/10.4271/2003-01-0631

[26] Pielecha I, Szwajca F, Skobiej K. Experimental investigation on knock characteristics from pre-chamber gas engine fueled by hydrogen. Energies. 2024;17(4):937. https://doi.org/10.3390/en17040937

[27] Qiang Y, Ji C, Wang S, Xin G, Hong C, Wang Z, Shen J. Study on the effect of variable valve timing and spark timing on the performance of the hydrogen-fueled engine with passive pre-chamber ignition under partial load conditions. Energ Convers Manage. 2024;302:118104. https://doi.org/10.1016/j.enconman.2024.118104

[28] Siano D, Panzam MA, D'Agostino D. Knock detection based on MAPO analysis, AR model and discrete wavelet transform applied to the in-cylinder pressure data: results and comparison. SAE Int J Engines. 2014;8(1):1-13. https://doi.org/10.4271/2014-01-2547

[29] Stępień Z. Analysis of the prospects for hydrogen-fuelled internal combustion engines. Combustion Engines. 2023. https://doi.org/10.19206/CE-174794

[30] Sun J, Zhang X, Tang Q, Wang Y, Li Y. Knock recognition of knock sensor signal based on wavelet transform and variational mode decomposition algorithm. Energ Convers Manage. 2023;287:117062. https://doi.org/10.1016/j.enconman.2023.117062

[31] Szwaja S, Bhandary K, Naber J. Comparisons of hydrogen and gasoline combustion knock in a spark ignition engine. Int J Hydrogen Energ. 2007;32(18):5076-5087. https://doi.org/10.1016/j.ijhydene.2007.07.063

[32] Szwaja S, Naber JD. Dual nature of hydrogen combustion knock. Int J Hydrogen Energ. 2013;38(28):12489-12496. https://doi.org/10.1016/j.ijhydene.2013.07.036

[33] Verhelst S, Sierens R, Verstraeten S. A critical review of experimental research on hydrogen fueled SI engines. SAE Technical Paper 2006-01-0430. 2006. https://doi.org/10.4271/2006-01-0430

[34] Wang K, Zhang Z, Sun B Zhang S, Lai F, Ma N et al. Experimental investigation of the working boundary limited by abnormal combustion and the combustion characteristics of a turbocharged direct injection hydrogen engine. Energ Convers Manage. 2024;299:117861. https://doi.org/10.1016/j.enconman.2023.117861

[35] White C, Steeper R, Lutz A. The hydrogen-fueled internal combustion engine: a technical review. Int J Hydrogen Energ. 2006;31(10):1292-1305. https://doi.org/10.1016/j.ijhydene.2005.12.001

[36] Yip HL, Srna A, Yuen ACY, Kook S, Taylor RA, Yeoh GH et al. A review of hydrogen direct injection for internal combustion engines: towards carbon-free combustion. Appl Sci. 2019;9(22):4842. https://doi.org/10.3390/app9224842

Filip Szwajca, MEng. – Faculty of Civil and Transport Engineering, Poznan University of Technology, Poland.
e-mail: *filip.szwajca@put.poznan.pl*

Cezary Gawrysiak, MEng. – Faculty of Civil and Transport Engineering, Poznan University of Technology, Poland.
e-mail: *cezary.gaw@gmail.com*

Prof. Ireneusz Pielecha, DSc., DEng. – Faculty of Civil and Transport Engineering, Poznan University of Technology, Poland.
e-mail: *ireneusz.pielecha@put.poznan.pl*